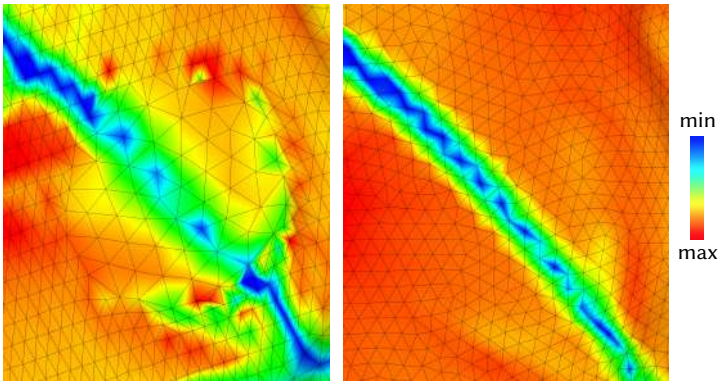


**Figure 5.17:** Estimating the Laplacian on an irregular (left) and regular (right) mesh: a poor tessellation may break the valleys of the Laplacian (discontinuous blue line) and introduce spurious local minima. Both types of artifacts may hinder the action of our filters, as exemplified in 5.16

depends on the location of the source, the geometry of the shape, and the discretization. Therefore, in general it is not possible to determine a priori which mesh density is suitable to detect all branches. The pruning policy needs an aggressive threshold to filter the branches ending at spurious local minima, also missing the weak branches of the cut locus (5.16, left). On the other hand, with the growing policy some branches of the cut locus are truncated too soon, because of bumps and cracks along the valleys of the Laplacian (5.16, middle). On a regular tessellation, both policies allow us computing an accurate estimate of the cut locus with reasonable thresholds (5.16, right).

At this regard, it is worth pointing out that the discrete Laplacian operator described in Section 3.2.2 turned out to be more resilient to irregular tessellation. Although even on regular tessellation the valleys slightly more evident with respect to the cotangent Laplacian (Figure 5.18, *left*), the difference is way more evident when computing the Laplacian of a distance field on the original Stanford bunny (Figure 5.18, *right*). Even if the branches are not identical in the two cases, since the tessellation are different and the source is not placed exactly in the same point, we can notice that our method still manage to clearly identify the main branches of the cut locus, while the cotangent method provides mostly weak branches that often blur away. Moreover, the presence of "false local minima" (isolated blue regions in the heat map of the bunny in the bottom-right of Figure 5.18) in this latter case may affect the expansion of the spanning tree, while, modulo the limitations discussed above, is more robust from this point of view.

We did not experiment with extreme cases characterized by very sparse meshing and long and skinny elements, such as many of the meshes found in the Thingi10k repository [ZJ16]. In that case, it may be convenient to use intrinsic triangulations [SSC19a] and related differential estimators [SC20b]. The rest of our method would work unchanged, but it needs being implemented in the framework of intrinsic triangulations.

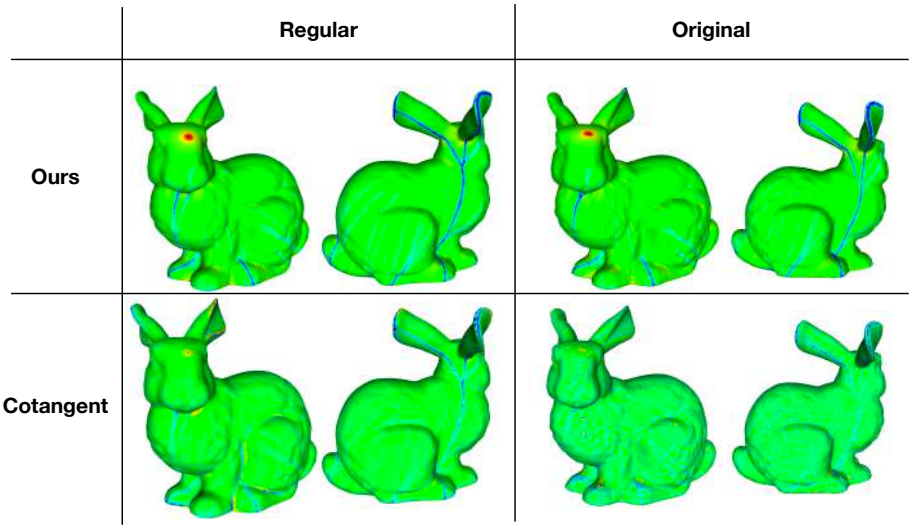


**Figure 5.18:** Estimation of the Laplacian with the operator described in Section 3.2.2 (*top*) and the cotangent Laplacian (*bottom*. On regular meshes (*left*), the performances of two methods is comparable, whereas on the original Stanford bunny our method demonstrate higher resilience to irregular tessellations.

## 5.6 Concluding remarks

We have presented a novel method to compute the cut locus that is practical and fast. The method depends on a unique intuitive parameter that can be tuned interactively to filter out artifacts arising from small details of the surface, or from discretization. The method works on surfaces of any genus, always recovering the correct topology of the cut locus; it works on shapes with sharp creases; and on rough shapes with many small details, too.

We conjecture that out method converges to the true cut locus as the mesh becomes denser, but proving this fact requires further work. In summary, all methods we adopted for computing the distance field can be shown to converge to the true geodesic distance; and the method to compute the differential quantities also converges for smooth functions. By applying such estimators to a denser and denser mesh, the estimated Laplacian should converge to the Laplacian of the distance function away from the cut locus, and to the Laplacian of a smooth barrier function near the cut locus. Thus, we expect that for any given value $A < 0$ there exists a mesh dense enough that $L(y) < A$ for all $y$ at the cut locus. However, since no bound from below to the Laplacian away of the cut locus is known, in general the Laplacian alone is not sufficient to characterize all and only the points of the cut locus. This fact further motivates the additional criteria that we apply in our method. We foresee two interesting avenues for future work. For the computation of the cut locus, we plan to improve on our current method to achieve a reliable fully automatic detection that works well in all practical scenarios. The most challenging issue in this direction is to determine where the weak free branches end. It would also be interesting to exploit the boundary structure provided by MMP-like algorithms,

as in [LCT11]. Based on such structure, the exact cut locus in the polyhedral metric can be computed. However, such a cut locus would consist of a dense tree, with one leaf at each parabolic vertex, thus being useful only for strictly polyhedral objects without any curved surface. It is an open problem how to define suitable pruning strategies to obtain a cut locus that is descriptive for curved objects approximated with a mesh, too.

Finally, we plan to explore the capabilities of our approach for the computation of the medial axis, which is a widely popular shape descriptor used for shape compression, matching and skeletonization [TDS+16]. Indeed, the medial axis can be defined as the cut locus of a distance field emanating from the boundaries of a geometric domain, growing inwards. Despite in this work we focused our attention on distance fields emanating from a single (point-like) source, in his work Générau showed that the Laplacian goes to $-\infty$ also for distance fields emanating from a general hypersurface embedded in the manifold domain [Gén20], creating a connection with the $\lambda$-medial axis [CL05]. In its current state, our algorithm is not able to reconstruct a proper connectivity for this more general case, but since the theoretical foundation still holds, it would be interesting to work at different tools to filter the Laplacian field and generate the medial connectivity, both for 2D and 3D manifolds.

# 6

# Vector Graphics on Surfaces Using Straightedge and Compass Constructions

**This section includes contents from a co-authored paper [MP22] that has been re-formatted for this thesis.**

## 6.1 Introduction

The ancient Greek mathematicians developed a set of geometric techniques, which go under the name of *straightedge and compass constructions*, to draw planar geometric figures. Such constructions do not require taking any explicit measure, they are granted by Euclid's first three postulates, and are based on two idealized tools: the straightedge, which can extend indefinitely the straight-line through any pair of points; and the compass, which can trace circles with its needle and pencil points at any two points in the plane. Besides, all intersections between straight lines and circles drawn with such tools can be found.

In the Euclidean setting, the straightedge and compass constructions can be substituted with simpler closed form solutions, though, as it is customary in 2D drawing systems. However, when addressing similar operations on a surface, one must rely on the computation of distance fields and geodesic lines. Such building blocks are indeed similar in nature to those available in the straightedge and compass framework. In the context of our effort to bring vector graphics to surface domains [MNPP22,NPP22], we thus investigate how to port such constructions to the manifold setting.

We address the problem with two complementary approaches. The first approach performs constructions in a tangent plane and then maps the result to the surface. The second approach extends the concepts of straightedge and compass to the geodesic metric and operates directly on the surface.

Euclidean constructions rely on properties that no longer hold under the geodesic metric, due to the intrinsic curvature of the surface. Because of that, both approaches fail in producing results that preserve *all* properties of their Euclidean counterpart. In fact, even the topological properties of straight lines and circles do not hold on a surface without additional conditions: geodesic lines may self-intersect or mutually intersect multiple times; and a generic

**Figure 6.1:** Examples of drawings obtained interactively with our prototype system on two meshes, each consisting of 1M triangles.

isoline of the distance field is not even guaranteed to be homeomorphic to a circle.

In order to address the topological limitations, we constrain our constructions to occur on sufficiently local subsets of the surface domain. Concerning the metric aspects, the first approach suffers from *geodesic distortion*, which is caused by the curvature when mapping Euclidean geometries from the tangent plane to the surface domain. On the contrary, geodesic lines and circles are well-behaved while working directly on the surface, as long as they the are "small enough". This fact increases our leeway in imposing some local properties.

We integrate all our constructions in a prototype system that supports interactive drawing with geodesic polygons and circles. We also support affine transformations of primitives and all the usual editing operations, such as copy, paste, and delete. We achieve real time interaction on meshes consisting of up to a few million triangles. This is made possible thanks to efficient algorithms to compute geodesic distances and shortest paths.

## 6.2 Related work

### 6.2.1 Intrinsic Geometry of Surfaces

The straightedge and compass constructions rely on basic theorems of the Euclidean geometry that relate lengths and angles. When trying to define similar relations on a surface, curvature must be taken into account. This subject was thoroughly investigated in the classical theory of intrinsic geometry of surfaces. See the books by Cheeger and Ebin [CE75] and by Chavel [Cha06] for comprehensive accounts. Referring just to the cases addressed in this paper, the local version of the Gauss-Bonnet theorem (Theorem 2.33) relates the internal angles of a geodesic polygon to the curvature of the region it encloses. Such

result explains the challenge in addressing constructions that require geodesic lines of given lengths *and* forming given angles. See, e.g., the isosceles triangle in 6.5.4.

Alexandrov investigated thoroughly the relations between quantities measured on a surface with their counterpart on surfaces with constant curvature (a.k.a. CAT – Cartan-Alexandrov-Topogonov – spaces) [Ale48]. In a nutshell, geodesic lines, which are cast from a common source along different directions, tend to converge if the curvature of the space is positive, and to diverge if it is negative. Based upon these facts, many comparison theorems involving Alexandrov and CAT spaces have been proposed in the literature. See Alexander et al. [AKP19] for a recent account on this subject; interestingly enough, the title of the chapter addressing geodesic triangles is *The ghost of Euclid*.

### 6.2.2 Vector Graphics

Vector graphics in 2D is a consolidated subject, supported in many systems and tools at industrial level [W3C10,Ado21,Ink21,Aut21,Pil21,Pix22]. Until recently, vector graphics on surfaces under the geodesic metric was considered too computationally expensive to be supported. Traditional methods to decorate a surface resort to parametrization and mapping, but this approach is prone to seams and distortion, as discussed by Nazzaro et al. [NPP22] and Yuksel et al. [YLT19]. The literature concerning tools for geodesic computations is vast, though, and has been recently surveyed by Crane et al. [CLPQ20]. Some recent contributions demonstrated that such technology is mature enough to support interactive editing directly on surfaces [MNPP22, NPP22, SC20a].

## 6.3 Basic Straightedge and Compass Constructions in the Plane

Straightedge and compass constructions involve just points, (segments of) straight lines, and (arcs of) circles in the Euclidean plane. They consist of iteratively applying the following five basic constructions:

- line through two existing points;
- circle through one point with center another point;
- intersection point of two non-parallel lines;
- intersection points of a line and a circle;
- intersection points of two circles.

Typical constructions usually start from few objects in the plane. In the most complex constructions – e.g., for polygons with many sides – the five operations above may be iterated many times, producing a number of intermediate objects, possibly much larger than the number of objects in the final result. Figure 6.2 illustrates the manifold counterparts of the five basic constructions

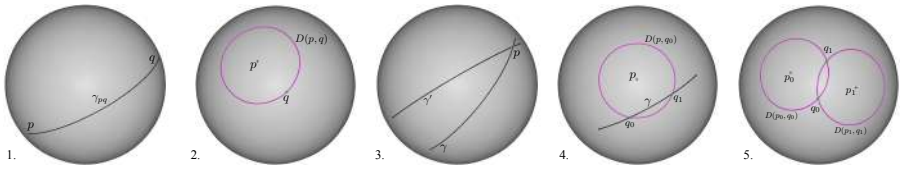


**Figure 6.2:** The five basic constructions on a sphere. The black curves are geodesic lines, while the curves in magenta are geodesic circles. We denote with $D(p, q)$ the geodesic circle centered at point $p$ and passing through point $q$.

on a sphere: straight-line segments are substituted with shortest geodesic paths; and circles are substituted with isolines of the distance field from a point.

### 6.3.1 The Geodesic Arsenal

Throughout the paper, we will rely on the following primitive operations to be performed on the surface $S$ under the geodesic metric. The implementation has been described in Chapter 3.

- *Geodesic-tracing:* given point $p \in S$ and a tangent direction $t \in T_pS$, trace a geodesic through $p$ with tangent vector $t$ at $p$; this is equivalent to a point-wise evaluation of the exponential map at $p$.
- *Tangent:* given a curve $\gamma$ on $S$ and one of its points $p$, return the direction $t \in T_pS$ tangent to $\gamma$ at $p$; if $\gamma$ is a geodesic line, this is indeed equivalent to a point-wise evaluation of the log map at $p$.
- *Shortest-path:* given points $p, q \in S$, return the shortest geodesic path $\gamma_{pq}$ connecting them;
- *Distance-field:* given $p \in S$, compute the distance field $d_p : S \longrightarrow \mathbb{R}$ where $d_p(q) := d(p, q)$;
- *Isoline:* given the distance field $d_p$ and a point $q \in S$ return the isoline of $d_p$ that goes through $q$;
- *Intersect:* given any two lines on $S$, not necessarily geodesic, return their intersection points.

In the context of 6.4, we will only rely upon the first three primitives, namely the point-wise evaluation of the exp and log map and the shortest path between two points. In Section 6.5 we will also make use of the other primitives, to reproduce the straightedge and compass tools directly on the surface $S$.

## 6.4 Constructions in Tangent Space

The constructions described in this section are based on the following idea: given an initial configuration of points of $S$, we use the log map centered at a suited point $c \in S$ to map such points onto the tangent space $T_cS$. We then

apply the Euclidean construction in $T_cS$, and finally map the result onto $S$ through $\exp_c$. In order to preserve topological consistency, we assume all the points involved in a construction to be contained in a convex ball centered at $c$. Some constructions may work on a large neighborhood as well, though.

Since $T_cS$ is a 2-dimensional vector space, we do not need any extension of the straightedge and compass tools. However, most of the properties of a given construction will be lost after applying the exponential map. Remarkably, this approach and the one described in Section 6.5 are somehow complementary: in many cases, the properties that one looses by using the former, can be preserved by using the latter, and vice-versa, Table 6.1 summarizes the results obtained with both approaches.

### 6.4.1 Operations with segments

Figure 6.3 shows some basic constructions in the Euclidean case, which are extended to the manifold setting in a straightforward way. These constructions are the only ones addressed in this paper, which are also insensitive to the method used to implement them. Everything works fine because they are based solely on distance and collinearity, whose properties are preserved in the manifold setting.

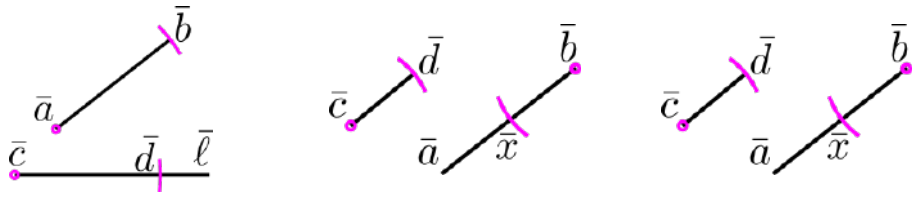


**Figure 6.3:** Transferring the length of a segment onto another one (*left*); adding two segments (*center*); and subtracting two segments (*right*).

Given a line segment $\bar{a}\bar{b}$ in the plane and a line $\bar{\ell}$ through another point $\bar{c}$, find a point $\bar{d}$ on $\bar{\ell}$ such that $\bar{a}\bar{b}$ and $\bar{c}\bar{d}$ have the same length. In the plane, the aperture of the compass is taken at $\bar{a}\bar{b}$, then the needle point is placed at $\bar{c}$ and a circle is traced; point $\bar{d}$ is taken at an intersection of the circle with line $\bar{\ell}$.[1] In the manifold case, we start with geodesic line segment $ab$ and a geodesic line $\ell$ on $S$. We first lift $b$ to a point $\bar{b}$ on the tangent plane $T_aS$ through the log map; likewise, we lift $\ell$ to a radial line $\bar{\ell}$ on $T_cS$. Then we use a standard compass to find the length of segment $\bar{a}\bar{b}$ on $T_aS$; and we use the same compass to draw a circle centered at $c$ on $T_cS$. We find the intersection between this circle and line $\bar{\ell}$; and finally we map the intersection point to $S$ with the exp map.

Given two line segments $\bar{a}\bar{b}$ and $\bar{c}\bar{d}$ in the plane, extend $\bar{a}\bar{b}$ at $\bar{b}$ for a length equal to $\bar{c}\bar{d}$. In the plane, segment $\bar{a}\bar{b}$ is extended to a line with the straightedge; the aperture of the compass is taken at $\bar{c}\bar{d}$ and a circle is traced by placing the needle point at $\bar{b}$; the intersection $\bar{x}$ of this circle with the line is taken,

1 We are assuming a non collapsible compass here; the same result can be also achieved with a collapsible compass, through a more involved procedure though.

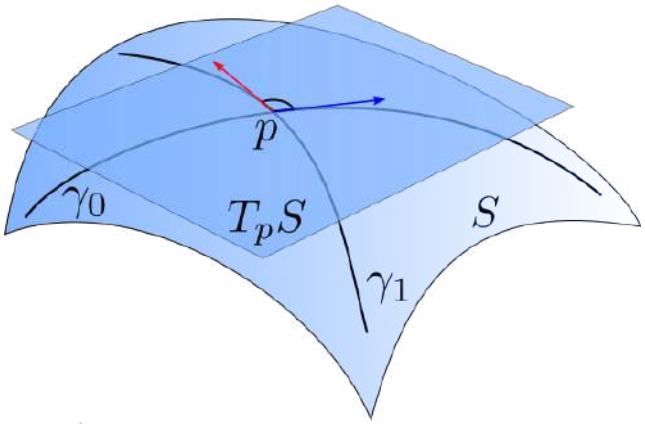


**Figure 6.4:** Two geodesic lines $\gamma$ and $\gamma'$ intersecting at point $p \in S$ form an angle defined by their tangents at $p$ on the tangent plane $T_pS$ (red and blue arrows)

which lies on the opposite side of $\bar{a}$ wrt $\bar{b}$; line segment $\bar{a}\bar{x}$ is the result. The construction in the manifold case is analogous to the previous and is omitted for brevity.

Given two line segments $\bar{a}\bar{b}$ and $\bar{c}\bar{d}$ in the plane, shorten $\bar{a}\bar{b}$ at $\bar{b}$ by the length of $\bar{c}\bar{d}$. In the plane, the aperture of the compass is taken at $\bar{c}\bar{d}$ and a circle is traced by placing the needle point at $\bar{b}$; the intersection $\bar{x}$ of this circle with $\bar{a}\bar{b}$ is taken; line segment $\bar{a}\bar{x}$ is the result. The construction in the manifold case is also analogous to the previous ones and is omitted for brevity.

### 6.4.2 Operations with angles

Let $\gamma_0$ and $\gamma_1$ be two geodesics intersecting at $p$; the angle between them at $p$ is defined from their tangent directions in the tangent plane $T_pS$. See Fig. 6.4 for an example.

In the plane, an angle is defined by two half-lines $\bar{\ell}_a$ and $\bar{\ell}_b$ incident at a point $\bar{c}$, which can be built with the straightedge, given two points $\bar{a}$ and $\bar{b}$ lying on them, respectively. This angle can be bisected as follows. Place the needle point of the compass at $\bar{c}$, trace any circle and let $\bar{p}$ and $\bar{q}$ be its intersections with $\bar{\ell}_a$ and $\bar{\ell}_b$. Place the needle point at $\bar{p}$, and next at $\bar{q}$, with aperture $\bar{p}\bar{q}$ trace another two circles; let $y$ be any of their two intersection points. The line $\bar{\ell}_y$ through $\bar{c}$ and $\bar{y}$ bisects the angle at $\bar{c}$. An additional property of the bisector is that all its points are equidistant from $\bar{\ell}_a$ and $\bar{\ell}_b$.

Analogously, given two geodesics $\gamma_{ca}$ and $\gamma_{cb}$ intersecting at $c$, we extend their tangent vectors at $c$ to lines $\bar{\ell}_a$ and $\bar{\ell}_b$ in $T_cS$, and use the Euclidean construction to find line $\bar{\ell}_y$ as above; then we map $\bar{\ell}_y$ to a geodesic $\gamma_{cy}$ emanating from $c$ and through $y = \exp_c(\bar{y})$. Line $\gamma_{cy}$ bisects the angle, in the sense that the angles formed by its tangent at $c$ and the tangents of the two input lines $\gamma_{ca}$ and $\gamma_{cb}$ at $c$ are equal, by construction. Figure 6.5 (left) illustrates this construction.

However, the points of $\gamma_{cy}$ in general will *not* be equidistant from the input

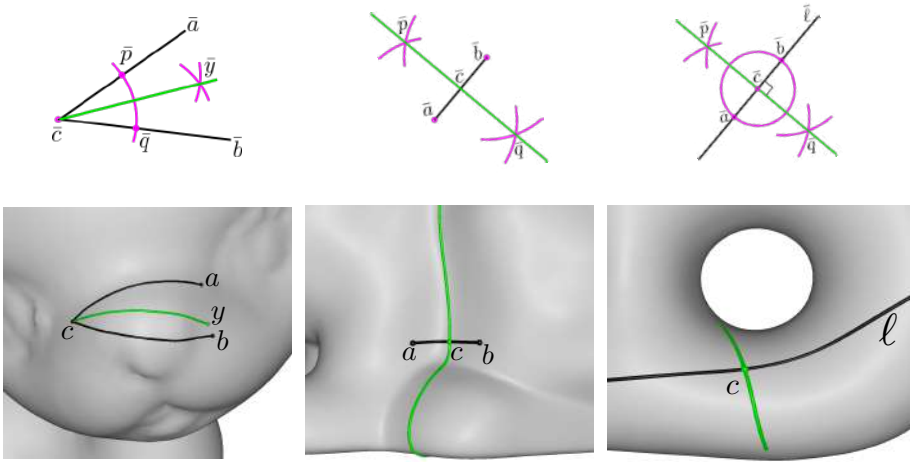


**Figure 6.5:** Euclidean constructions of the angle bisector(*top left*), segment bisector (*top center*) and perpendicular to a line at a point (*top right*). The corresponding constructions in the manifold case (*bottom*) are obtained by mapping the lines, which are obtained with the Euclidean constructions in the tangent plane at $c$, to $S$ through the exp map.

lines. In fact, the locus of equidistant points from the two lines is not a geodesic line in general, and finding it is beyond the scope of this paper, as it requires using the distance fields from $\gamma_{ca}$ and $\gamma_{cb}$, while we limit our distance fields to have their sources at single points (see Section 6.3.1).

A number of other constructions deal with operations on angles, such as copying an angle, adding or subtracting angles, or creating angles of a few specified amplitudes. These problems are somehow local to the point $c$ at the tip of the angle, and can be addressed by finding the tangents of the geodesic lines that define the angles at play, resolving the Euclidean construction in the tangent plane, and using the resulting directions to map the geodesics to the surface $S$. For this reason, we do not analyze such constructions in detail.

### 6.4.3 Perpendicular to a line and the Square-set operator

#### Perpendicular bisector and midpoint

In the plane, the bisector is constructed as follows. Given points $\bar{a}, \bar{b} \in \mathbb{R}^2$, first use the straightedge to trace the straight-line segment joining them. Then place the needle point of the compass at $\bar{a}$ and the pencil point at $\bar{b}$ and trace a circle; repeat the same operation with needle at $\bar{b}$ and pencil at $\bar{a}$. Let $\bar{c}, \bar{d}$ be the intersection points of the two circles; use the straightedge to trace segment $\bar{c}\bar{d}$. The *straight line* line through $\bar{c}, \bar{d}$ intersects segment $\bar{a}\bar{b}$ *orthogonally* and *at its midpoint* $\bar{c}$; this is also the *locus of points that have equal distance* from $\bar{a}$ and $\bar{b}$. The Euclidean construction is depicted at the top of Figure 6.5(middle).

Let now $a, b$ be two points in $S$ and let $\gamma$ be the shortest geodesic connecting them. We cannot apply the Euclidean construction in either tangent plane $T_aS$ or $T_bS$ and then map the result to $S$, as it would not have any of the above

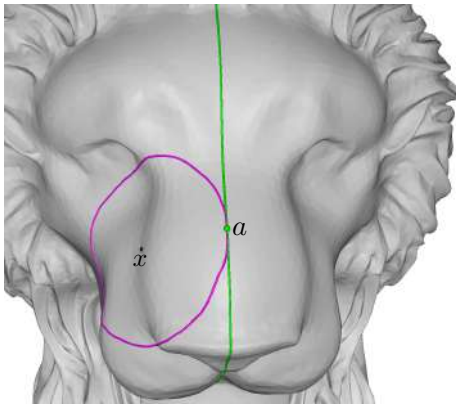


**Figure 6.6:** Line tangent to a circle centered at $x$ and through $a$: the square set is placed at $a$ and oriented according to the tangent of $\gamma_{xa}$ at $a$.

properties in general, and we would also obtain different results in the two cases. We rather apply the Euclidean construction in tangent plane $T_cS$, where $c$ is the midpoint of $\gamma$. In order to find $c$, we first find point $\bar{c}$ in the Euclidean construction on $T_aS$ and we map it to $S$ through the exp map; $c$ is the midpoint of $\gamma$ by construction. Now we consider the tangent $t_c$ of $\gamma$ at $c$, and we proceed as before to find the vector $t_c^{\perp}$ orthogonal to $t_c$. The result $\gamma^{\perp}$ is the geodesic line tangent to $t_c^{\perp}$ at $c$. The result is shown at the bottom of Figure 6.5 (middle).

Note that this construction satisfies just two of the three propertie of its Euclidean counterpart, since our result it is not the locus of points equidistant from $a$ and $b$. In Section 6.5.2 we propose a method that constructs a curve whose points satisfy this last property, without being a geodesic though.

### Perpendicular to a line at a point

In the plane, let $\bar{\ell}$ be a line and $\bar{c}$ a point on it, we want to find a line through $\bar{c}$ and orthogonal to $\bar{\ell}$. To this aim, it is sufficient to trace any circle centered at $\bar{c}$, finding its intersections $\bar{a}, \bar{b}$ with $\bar{\ell}$, and then finding the bisector of line segment $\bar{a}\bar{b}$.

Such construction can be ported to the manifold setting as above. The advantage in this case is that we already know the position of $c$ on the geodesic $\gamma$, so we just work in $T_cS$. Fig. 6.5 (right) shows both constructions. The same method can be used to find the tangent at a point $a$ to a circle centered at $x$ and through $a$. This is in fact the perpendicular to geodesic segment $ax$ and passing through $a$. Fig. 6.6 shows such construction.

### The Square-set as derived operator

Given a curve $\gamma$ on $S$ and a point $c$ on it, the above construction can be used to compute the vector $t^{\perp} \in T_cS$ orthogonal to the tangent $t_c$ of $\gamma$ at $c$. This procedure implements an operation that we call *Square-set*, which will be used as an atomic operation in the following.

### 6.4.4 Regular Polygons

In the Euclidean setting, the construction of a regular $n$-gon boils down to construct a straight line segment of length $\cos(\frac{2\pi}{n})$. If one starts with two points $O, e$ on the plane, and set the length of the straight line segment $Oe$ to be 1, then it is well known that a segment of length $\ell$ is constructible using straightedge and compass if and only if $\ell$ can be obtained from 1 using the operations $+, -, \cdot, \div$ and $\sqrt{\cdot}$. By the law of cosines, we have that the side of an $n$-gon inscribed in the unit circle centered at $O$ has length $d = \sqrt{2 - 2\cos(2\pi/n)}$. Hence, if we can construct a segment of length $\cos(\frac{2\pi}{n})$, then $d$ is constructibile. In 1796, Gauss stated a sufficient condition for $\cos(\frac{2\pi}{n})$ to be constructible, and in 1837 Pierre Wantzel proved that such condition is also necessary. The final result states that a regular $n$-gon can be constructed with straightedge and compass if and only if $n$ is of the form

$$n = 2^j \cdot p_1 \cdot p_2 \cdots p_m,$$

where $p_i$ is a prime number of the form $p_i = 2^{2^{k_i}} + 1$, $k_i \in \mathbb{N}$, for all $i = 1, \ldots, m$. Once a chord of length $d$ has been constructed, then we can use the compass to transfer such length $n - 1$ times on the circle. Of course, the result will be a regular $n$-gon because we are just duplicating the triangle of vertices $(0,0), (1,0), (\cos(\frac{2\pi}{n}), \sin(\frac{2\pi}{n}))$ $n - 1$ times. Note that, since $\sin(\alpha)^2 = 1 - \cos(\alpha)^2$, the constructability of $\cos(\alpha)$ implies the one of $\sin(\alpha)$.

In the manifold case, given two points $c, v_1 \in S$, if $r$ is the length of the geodesic connecting them, then the above construction can be used to determine the $n$ vertices $\{\bar{v}_1, \ldots, \bar{v}_n\} \in T_pS$ of a regular $n$-gon, and then define $v_i := \exp_p(\bar{v}_i)$ for $i = 1, \ldots, n$. In fact, since $T_pS$ is a 2-dimensional vector space, we can define a system of coordinates having $c$ as origin, an putting $\bar{v}_1 = log_c(v_1) = (0, r)$. Then the final result can be obtained by connecting $v_i$ to $v_{i+1}$ with shortest paths, for $i = 1, \ldots, n$ (here and in the folllowing, we implicitly mean that the subscripts have to be considered modulo $n$). In this way, we are constructing a geodesic $n$-gon which satisfies just two of the properties of its Euclidean counterpart: if $t_i \in T_pS$ is the tangent of the radial geodesic $\gamma_i$ connecting $c$ with $v_i$ at $c$, then the angle formed by $t_i$ and $t_{i+1}$ is $\frac{2\pi}{n}$, and the length of $\gamma_i$ is $r$, $i = 1, \ldots, n$. We will see that the former property is ensured by construction and the definition of angle given in Section 6.4.2 and the latter is a consequence of the fact the exponential map is a radial isometry (see Section 2.2).

The first advantage of retrieving the points $\{v_1, \ldots, v_n\}$ through a construction that takes place in $T_pS$ is that such points will be always defined. Nervetheless, the topological correctness of the result depends on the radius of injectivity of $p$ (think about the case of a cylinder of radius $R$ and $r \geq 2R$). Moreover, this method seems well suited to define affine transformations. In fact, rotation by angle $\theta$ and scaling by a factor $\lambda$ can be applied in $T_cS$ by choosing $\bar{v}_1 = (\cos(\theta), \sin(\theta))$ and by multiplying $r$ by $\lambda$. Also translation is straigtforward: it suffices to parallel transport the vector $\bar{v}_1 \in T_cS$ to $T_{c'}S$ along a shortest path connecting $c$ to $c'$ and then repeat the construction in $T_{c'}S$,

where $c'$ is another point on $S$. The details on the implementation of such operations are given in Section 6.7.

We will now describe the constructions implemented in our drawing system. There are many straightedge and compass constructions for regular polygons, We limit ourselves to describe the Euclidean constructions and presenting the results obtained by mapping such constructions on $S$ as described above. Details about the implementation of the exponential mapping and shortest paths tracing will be given Section 6.7. From now on, $r$ will denote the length of the geodesic $\gamma(t)$ connecting two fixed points $c, v_1 \in S$. All the constructions below will take place the tangent plane $T_cS$, within which we define a system of coordinates having $c$ as origin, the straight line having $log_c(v_1)$ as tangent at the origin as $x$-axis, and the perpendicular to such line at $\bar{c} = (0, 0)$ as $y$-axis. In such a reference frame, we define $\bar{v}_1 := (r, 0)$ and we denote with $C$ the circle centered at $\bar{c}$ with radius $r$.

EQUILATERAL TRIANGLE Let $\bar{v}_1, \bar{v}_1'$ be the points at which $C$ intersect the $x$-axis, i.e $\bar{v}_1 = (r, 0)$ and $w = (-r, 0)$. Place the compass at $w$ and trace a circle with radius $r$. Let $\bar{v}_2, \bar{v}_3$ be the intersections of such circle with $C$. Then $\{\bar{v}_1, \bar{v}_2, \bar{v}_3\}$ is an equilateral triangle.

SQUARE By proceeding as above, we construct two points $\bar{v}_1 = (r, 0)$ and $\bar{v}_3 = (-r, 0)$. The points $\bar{v}_2$ and $\bar{v}_4$ are the intersection of $C$ with the $y$-axis, i.e $\bar{v}_2 = (0, r)$ and $\bar{v}_3 = (0, -r)$.

PENTAGON Let $\bar{v}_1 = (r, 0)$, $\bar{v}_1' = (-r, 0)$ and $\bar{s} = (0, r)$ constructed as above. Let $\bar{m}$ be the midpoint of the line segment $\bar{s}\bar{c}$. Place the needle of the compass at $\bar{m}$ and the pencil at $\bar{s}$ and trace a circle. Let $\bar{n}_0, \bar{n}_1$ be the intersection of such circle with the line through $\bar{v}_1'$ and $\bar{m}$. W.l.o.g, we assume $\bar{n}_0$ to be the closest one to $\bar{v}_1'$, and let us denote with $r_i$ the distance between $\bar{v}_1'$ and $n_i$, $i = 0, 1$. Let $C_i$ be the circle centered at $\bar{v}_1'$ with radius $r_i$, $i = 0, 1$. Then $\{\bar{v}_3, \bar{v}_4\} = C_0 \cap C$ and $\{\bar{v}_2, \bar{v}_5\} = C_1 \cap C$.

HEXAGON Let $\bar{v}_1 = (r, 0)$ and $\bar{v}_4 = (-r, 0)$ constructed as above. Place the needle at $\bar{v}_1$ and trace a circle of radius $r$. Let $\bar{v}_2, \bar{v}_6$ be the intersections of such circle with $C$. Place the needle at $\bar{v}_4$ and construct $\bar{v}_3, \bar{v}_5$ in the same way. Then $\{\bar{v}_1, \bar{v}_2, \ldots, \bar{v}_4\}$ is a regular hexagon.

OCTAGON Once a square is constructed as described above, an octagon can be obtained by intersecting the angle bisector of every quadrant with $C$.

DECAGON Proceed as in the construction of the pentagon until the circle centered at $\bar{m}$ through $\bar{s}$ is traced. Let $\bar{n}$ the intersection with such circle with the straight line segment connecting $\bar{v}_1$ with $\bar{m}$. Let $r_1$ be the length of the segment $\bar{n}\bar{v}_1$ on $C$. Then the vertices $\bar{v}_2$ and $\bar{v}_{10}$ are the intersections of the circle $C_1$ centered at $\bar{v}_1$ with radius $r_1$ with $C$. The other vertices can be found

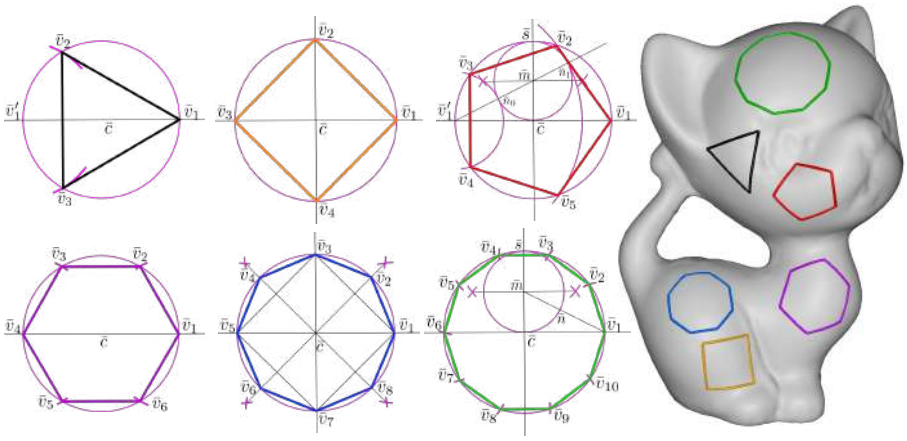

**Figure 6.7:** Euclidean construction of an inscribed regular $n$-gon for $n = 3, 4, 5, 6, 8, 10$ (*left*) and the results obtained by mapping such constructions on a mesh (*right*).

by iteratively intersecting a circle with the same radius $r_1$, centered at vertices found at the previous iteration.

Figure 6.14 summarizes the constructions described in this section both in the Euclidean and in the manifold setting.

### 6.4.5 Parallelogram, rhombus and rectangle

With the notations used in the previous section, let $\bar{v}_1 = (r, 0)$ and $\bar{v}_3 = (-r, 0)$. Place the needle at the origin and trace any circle, which we will denote with $\widehat{C}$. Pick any point $\bar{v}_2$ on $\widehat{C}$ and consider the line through $\bar{v}_2$ and $\bar{c}$. If $\bar{v}_4$ is the other point at which this line intersects $\widehat{C}$ then $\boldsymbol{Q} := \{\bar{v}_1, \bar{v}_2, \bar{v}_3, \bar{v}_4\}$ is a parallelogram.

Note that if $\bar{v}_2 = (0, R)$, with $R$ being the radius of $\widehat{C}$, then $\boldsymbol{Q}$ is a rhombus, while if $\bar{v}_2$ does not lie on the $y$-axis but $R = r$, then $\boldsymbol{Q}$ is a rectangle. In the particular case in which $\bar{v}_2 = (0, r)$ then $\boldsymbol{Q}$ is a square. See Figure 6.8.

Also in this case, we have no guarantees of equal length of opposite sides or equal angles at opposite corners; let alone the notion of "parallel sides", which is ill defined on a manifold. The only guarantee is that opposite semi-diagonals lie on a geodesic through $c$ and have equal lengths, and, consequently, opposite angles at the center are equal. The rhombus has the additional property that the diagonals are orthogonal. And the rectangle has all four semi-diagonals with the same length.

In summary, all constructions above can guarantee only properties related to lengths and angles that depend just on the radial geodesics emanating from the center $c$, at which the tangent plane is placed. This is a consequence of the fact the exponential map is a radial isometry, and that the angles between two geodesics are defined in the tangent space of their interesection. Note that the sides of the geodesic polygons are traced only *after* their corners have been mapped to $S$ through the exp map. The length of such lines, as well as the angles they form at the corners, are influenced from the Gaussian curvature

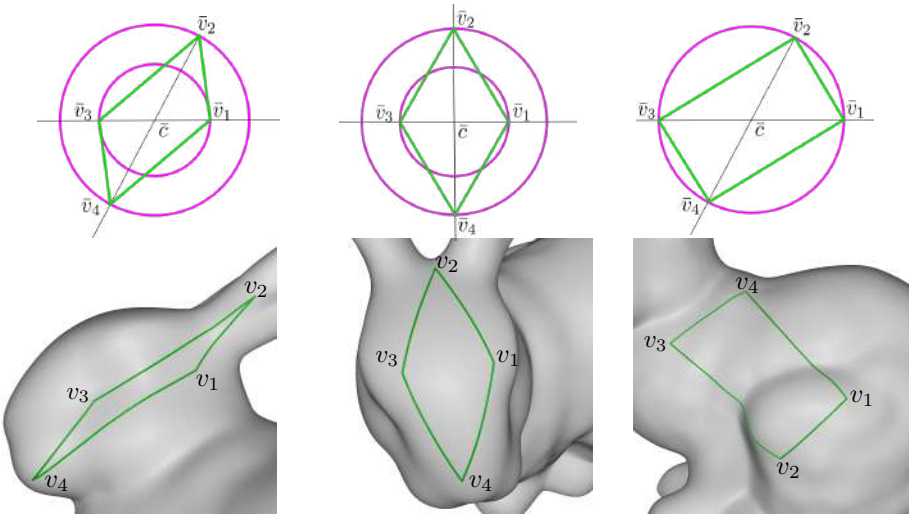


**Figure 6.8:** Euclidean constructions of a parallelogram, a rhombus and a rectangle (*top*) and the results obtained by mapping such constructions to a mesh (*bottom*).

of $S$ in the region covered by the polygon: the more the Gaussian curvature around $c$ varies, the more the shape of the geodesic polygon will differ from its Euclidean counterpart.

### 6.4.6 Remarks

Overall, the constructions of inscribed polygons cannot ensure any property concerning the length of their sides as well as their internal angles. However, some considerations can be made about both quantities in order to understand how much the curvature of the surface affects the shape of a regular $n$-gon obtained with the above constructions. For the sake of brevity, we restrict ourselves to a high-level discussion, with the purpose of just giving an idea of what kind of results may be used to better understand how the shape of our polygons may be influenced by the curvature around the center $c$. For more details about such result, we refer to [CC89, pages 197-198] and [Ber07, Sec. 6.4].

With the notations used above, let consider two points $\bar{v}_1, \bar{v}_2 \in T_c\mathcal{M}$ picked on the circle $C$ centered at $\bar{c}$. Let $T$ be triangle having vertices $\{\bar{c}, \bar{v}_1, \bar{v}_2\}$ and $\mathcal{T}$ the one having vertices $\{c, v_1, v_2\}$. Then both $T$ and $\mathcal{T}$ have two sides of length $r$ and the angle formed by such sides is equal to $2\pi/n$. However, $T$ is a plane triangle, while $\mathcal{T}$ is not. So one could say that the all the differences between these two triangles are somehow localized in the length $\ell$ of the geodesic connecting $v_1$ to $v_2$ and in the angles $\alpha_1, \alpha_2$ at such vertices. For what said in Section 2.3.2, it is clear $\ell$ depends on how much $\exp_c$ fails in being an isometry, and, therefore, it can be estimated by considering a Jacobi field along $\gamma_{cv_1}$. In the case of manifolds with constant curvature, Jacobi fields have a closed form, which have been used to prove the well known *Toponogov triangle comparison theorem*.

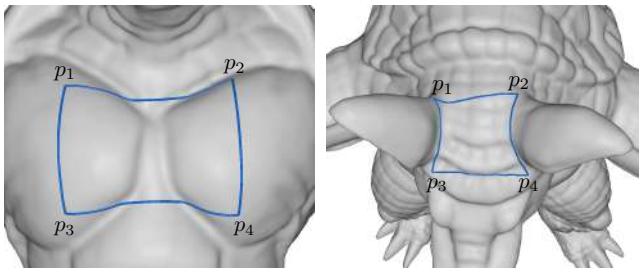


**Figure 6.9:** Two examples of squares drawn in bumpy regions of a mesh. In some cases, the geodesic distortion is more evident when the length of the sides is considered (left), in other instances we better notice it by looking at the angles (right).

After introducing some notations, we will state this latter result in our specific setting and refer to [Ber07] for further details about this subject. In the following, we assume $r < r_p$. If $K$ denotes the Gaussian curvature on $S$, let us put

$$\delta := \inf K \qquad \Delta := \sup K,$$

and let us denote with $S(\sigma)$ the surface having constant curvature $\sigma$. Let $T_\delta$ and $T_\Delta$ be the triangles with vertices $\{c', v_1', v_2'\} \in S(\delta)$ and $\{c'', v_1'', v_2''\} \in S(\Delta)$, respectively. Suppose these triangles have two sides of length $r$ and the angle between such sides is $2\pi/n$. Then, by the Toponogov triangle comparison theorem we have

$$d_{S_\Delta}(v_1'', v_2'') \leq \ell \leq d_{S_\delta}(v_1', v_2'),$$

where $d_{\mathcal{M}}(\cdot, \cdot)$ denotes the geodesic distance measured with the metric of the manifold $\mathcal{M}$. This means that the more $K$ varies around $c$, the more $\ell$ could differ from $\|v_2 - v_1\|$. Concerning the angles at $p_1$ and $p_2$, by re-writing (2.23) for the case $k = 2$ we have that

$$\sum_{i=1}^{3} \alpha_i = \iint_{\mathcal{T}} K d\sigma + \pi,$$

where $\alpha_0, \alpha_1, \alpha_2$ are the angles at $c, v_1, v_2$, respectively. This means that the sum of the internal angles of $\mathcal{T}$ differs from $\pi$ by an amount which is equal to the integral of the curvature in its interior. To fix ideas, one can think about the case in which $\mathcal{M}$ is a unit sphere. Then $K \equiv 1$ and the above formula tells us that the excess of $\sum_{i=1}^{3} \alpha_i$ over $\pi$ is equal to the area of $\mathcal{T}$.

Summarizing the above considerations, we can say that the more the surface is far from being flat, i.e. the more the Gaussian curvature is great in norm, the more the shape of $\mathcal{T}$ would differ from the one of its Euclidean counterpart $T$. Figure 6.9 show two examples of two squares drawn in bumpy regions of a mesh, which look very different from the one shown in Figure 6.7.

## 6.5 Direct Constructions on the Surface

We now change approach, by defining the equivalent tools for the straightedge and compass directly on $S$. Referring to the geodesic arsenal defined in Section

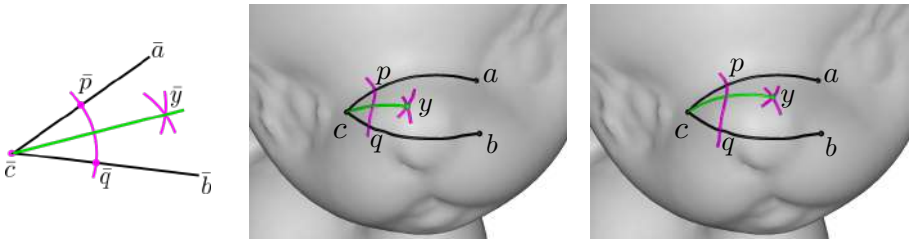


**Figure 6.10:** The Euclidean construction to bisect an angle (*left*) fails when ported to a surface: the resulting lines (*center* and *right*) do not bisect the angle at $c$ and they are different depending on the choice of points $p$ and $q$.

6.3, the operator *Shortest-path* allows us to trace geodesic segments between any two endpoints; and the joint use of *Tangent* and *Geodesic-tracing* allows us to extend such a segment indefinitely from both sides. We thus define the derived operation *Geodesic-line* that traces an arbitrarily long line through a pair of points, generalizing the straightedge to the manifold setting.

Likewise, the *Geodesic-compass* is a derived operation defined as the *Isoline* through a given point of the *Distance-field* from another center point. Note that, the *Distance-field* alone does not belong to the straightedge and compass framework, because it implicitly takes measures. On the other hand, since this operator is anyhow necessary to implement the *Geodesic-compass*, we will use it also directly to address constructions where the basic tools fail.

We address the five basic constructions listed in Section 6.3 by means of *Geodesic-line* (1); *Geodesic compass* (2); and *Intersect* (3, 4, 5), as depicted in Figure 6.2. Besides, we will make use of the *Square-set* operator, as defined in Section 6.4.3.

Since we need topological consistency between the result of our constructions on $S$ and their Euclidean counterpart, we will always assume that we are considering strongly convex objects in the sense of Section 2.4.

In the following, we review some straightedge and compass constructions, showing their extension to the manifold setting with this approach, as an alternative to the constructions in tangent plane presented in the previous section. Again, we will see that these constructions can preserve only some of the properties that are guaranteed in the Euclidean case.

### 6.5.1 Angle bisection

The Euclidean construction depicted in Figure 6.5 (top-left) fails when ported to a surface with our geodesic tools. See Fig. 6.10. The geodesic line through $c$ and $y$ neither bisects the angle at $c$, nor its points are equidistant from the input lines. Moreover, the result depends on the radius chosen to find $p$ and $q$.

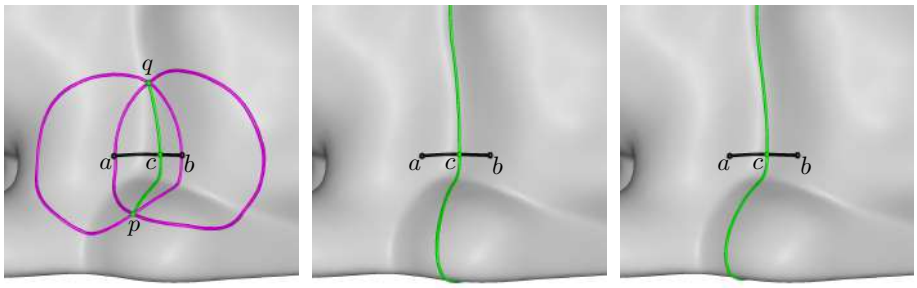


**Figure 6.11:** The bisector of a geodesic segment computed by reproducing the Euclidean construction (*left*); by the zero isoline of the difference of distance fields from $a$ and $b$ (*center*); and by tracing a geodesic from the midpoint of the segment along the orthogonal direction computed with the *Square-set* (*right*). The last construction is equivalent to the one in Section 6.4.3.

### 6.5.2 Line segment bisector and midpoint

The Euclidean construction described in Section 6.4.3 also fails on a surface. If we use *Geodesic-line* and *Geodesic-compass* to obtain points $p, q$, the two geodesic paths $\gamma_{ab}$ and $\gamma_{pq}$ in general will not intersect at the midpoint of $\gamma_{ab}$, nor they will be orthogonal at $c$. Concerning distances, we only know that $p$ and $q$ are equidistant from $a$ and $b$, but distances can be different at all other points of $\gamma_{pq}$. See Figure 6.11 (left).

We thus resort to our additional tools. Let $d_a, d_b$ be the two distance fields with sources at $a$ and $b$, respectively. Compute the difference field $d_{ab} = d_a - d_b$; the point $p$ computed before belong to the zero isoline of this field. If we extract the *Isoline* of $d_{ab}$ through $p$, the resulting line $\gamma_{ab}^{\perp}$ will intersect orthogonally $\gamma_{ab}$ at its midpoint. See Figure 6.11 (center). This construction has the further property, which we did not have with the construction in Section 6.4.3, that all points of $\gamma_{ab}^{\perp}$ are equidistant from $a$ and $b$. However, $\gamma_{ab}^{\perp}$ is not a geodesic line, hence not *straight* in the manifold sense. Finally, the construction presented in Section 6.4.3 can be replicated by first finding the midpoint $c$ of geodesic $\gamma_{ab}$, as above, and then applying the *Square-set* operator at $c$ to find the perpendicular line. See Figure 6.11 (right).

### 6.5.3 Circle through three non-collinear points

In the plane, given three non-collinear points $\bar{a}, \bar{b}, \bar{c}$, this construction can be done by first computing the perpendicular bisectors of segment $\bar{a}\bar{b}$ and $\bar{b}\bar{c}$; then intersecting such two bisectors at point $\bar{o}$; and finally tracing the circle centered at $\bar{o}$ and through $\bar{a}$ (and, consequently, through $\bar{b}$ and $\bar{c}$). See Figure 6.12(left). The same procedure trivially gives the circle circumscribed to a triangle $\bar{a}\bar{b}\bar{c}$.

This construction relies on the fact that all points on a bisector are equidistant from the endpoints of the input segment, a property which is not fulfilled in the manifold case when the bisector is a straight line, as in Figure 6.12(middle).

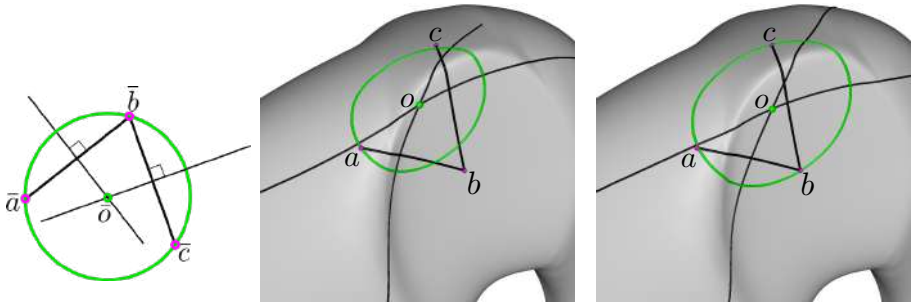


**Figure 6.12:** Euclidean constructions of a circle through three points $a, b, c$ (*left*). A straightforward reproduction of the Euclidean construction fails because the intersection $o$ of the two thin black lines is not equidistant from $a, b, c$ (*center*). The intersection of curves obtained as isolines of the difference distance fields from pairs of points gives the correct center of the geodesic circle (*right*).

However, if the two bisectors are obtained as isolines of the difference distance field, as described above, then their intersection will indeed be equidistant from the three points, hence we can use it as the center for a geodesic circle through them. See Figure 6.12(right).

Note that this construction cannot be replicated while working in tangent space, because one would need to know the center $o$ of the circle in advance.

### 6.5.4 Polygons

We already observed that the constructions in Section 6.4.4 and Section 6.4.5 do not ensure any property concerning the length of the sides and/or the amplitude of the internal angles of the resulting polygons. We now address some of those properties with direct constructions on $S$. To this aim, we rely on different Euclidean constructions, which do not work inside a circle.

#### Triangles

A triangle can be copied to another place with the same construction, both in the planar and in the manifold setting. Let $\bar{a}\bar{b}\bar{c}$ be a triangle, $\bar{\ell}$ a line and $\bar{a}'$ a point on $\bar{\ell}$. We want to copy the triangle in such a way that $\bar{a}$ goes to $\bar{a}'$, $\bar{b}$ goes to a point $\bar{b}'$ on $\bar{\ell}$, and $\bar{c}$ is placed at a point $\bar{c}'$ accordingly. We first draw a circle with amplitude $\bar{a}\bar{b}$ centered at $\bar{a}'$ and we select a point $\bar{b}'$ as one of the two intersections of the circle with line $\bar{\ell}$. Next we trace two more circles, one with amplitude $\bar{a}\bar{c}$ centered at $\bar{a}'$ and another with amplitude $\bar{b}\bar{c}$ centered at $\bar{b}'$; we select point $\bar{c}'$ as one of the intersections of such two circles. In the manifold setting, the result is a triangle with edges of the same length of $abc$, but nothing can be said about its angles. Moving a triangle while preserving the amplitude of its angles is inherently impossible in general, for consequences of the Gauss-Bonnet theorem.

Creating an equilateral triangle is among the simplest constructions: given an edge $\bar{a}\bar{b}$, intersect the two circles with radius $\bar{a}\bar{b}$ and centered at $\bar{a}$ and $\bar{b}$,

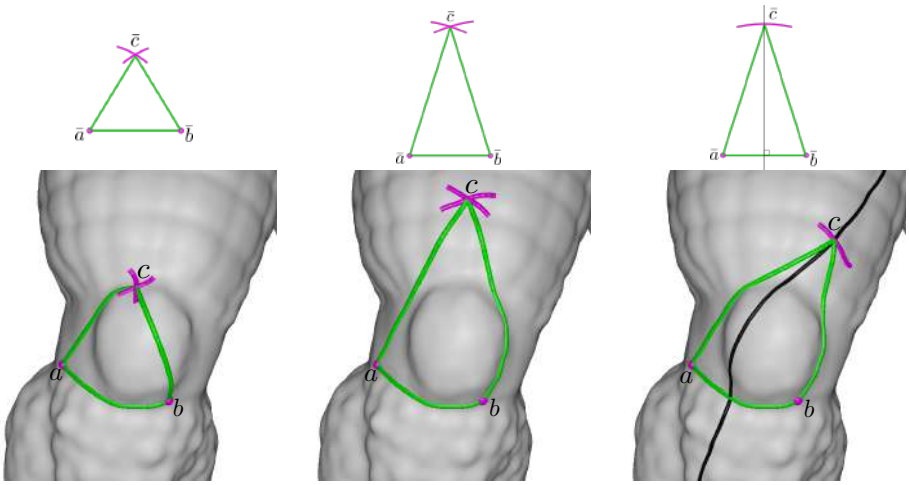


**Figure 6.13:** Straightedge and compass constructions of an equilateral (*left*) and isosceles triangle given the length of the sides (*center*) and the height (*right*) in the Euclidean (*top*) and manifold setting (*bottom*).

respectively. Any of their two intersections can be chosen as the third vertex $\bar{c}$ of the triangle. The same procedure works in the manifold setting too, if we aim at obtaining a triangle with three edges of the same length. This does not guarantee any other of the properties of the equilateral triangles, e.g., having three equal angles, having three equal heights that bisect the angles and bisect the edges, etc. Constructions fulfilling even one of such requirements seem not easy to obtain in the manifold setting.

Likewise, it is easy to build an isosceles triangle on a basis $\bar{a}\bar{b}$ with the diagonal edges of a given length (transferred with the compass from some given segment). Alternatively, one can build an isosceles triangle of a given height, by first constructing the perpendicular bisector of $\bar{a}\bar{b}$ and then transferring the height on it with the compass. Both such constructions work to some extent in the manifold setting, too. However, the first construction will not warrant anything about either equality of the angles at the basis, or the height from $c$ to bisect $ab$. While the second construction will just warrant the latter property, but neither that the diagonal edges, nor that the angles at the basis are equal. In our system, we implemented a more practical, yet equivalent, variant of the first construction: we consider the *Isoline* of points equidistant from $a$ and $b$, as in Section 6.5.2, and we let the user choose the length of the sides by dragging point $c$ along such bisector. Figure 6.13 (bottom) shows Euclidean constructions for equilateral and isosceles triangles, together with their counterparts on a surface.

### Squares and rectangles

A square can be built from one of its edges $\bar{a}\bar{b}$ as follows. A line perpendicular to $\bar{a}\bar{b}$ and through $\bar{a}$ is built first. Then the the length of $\bar{a}\bar{b}$ is transferred to segment $ad$ on such a line by placing the needle point of the compass at $\bar{a}$.

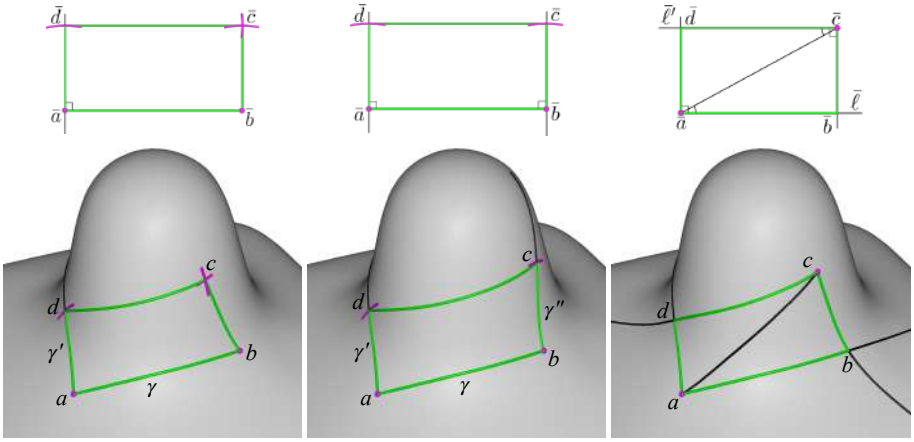


**Figure 6.14:** Rectangles obtained with different constructions: by tracing two perpendicular lines $\gamma$ and $\gamma'$ intersecting at $a$ and tracing opposite sides of the same length (*left*); by tracing two lines $\gamma'$ and $\gamma''$ perpendicular to $\gamma$ at $a$ and $b$ and setting points $d$ and $c$ on $\gamma'$ and $\gamma''$ at equal distance from $a$ and $b$, respectively (*center*); by tracing the diagonal $ac$, transferring angle $bac$ to $acd$ and tracing two lines perpendicular to $ab$ and $cd$ at $a$ and $c$, respectively (*right*). The constructions are shown both in the Euclidean (*top*) and in the manifold (*bottom*) setting.

Finally, the needle point of the compass is placed at $\bar{b}$ and at $\bar{d}$ with the same aperture $\bar{a}\bar{b}$, and the intersection $\bar{c}$ of the two circles gives the last vertex of square $\bar{a}\bar{b}\bar{c}\bar{d}$.

This same construction works in the manifold setting too. However, the resulting polygon will have four edges of equal length, but only angle $d\hat{a}b$ is guaranteed to be a square angle. An alternative construction consists of tracing perpendicular lines at both $a$ and $b$, by means of the *Square-set*, transferring the length of $ab$ on both of them, and connecting the points $c$ and $d$ obtained in this way. In this case, in the manifold setting we obtain a quadrilateral with three edges of the same length, namely $ab$, $ad$ and $bc$, and two right angles $d\hat{a}b$ and $a\hat{b}c$; but nothing can be said about the length of edge $cd$ and the amplitude of angles at $c$ and $d$.

The same constructions apply to draw a rectangle, except that the aperture of the compass to obtain the vertical edges can be different than the length of $ab$. The outcome in the manifold setting has the analogous (lack of) properties.

We describe a third construction, which is more appropriate to the GUI of drawing systems. Given a basis line $\bar{\ell}$ and a point $\bar{a}$ lying on it, a diagonal segment $\bar{a}\bar{c}$ is traced first. Then the angle between such segment and line $\bar{\ell}$ is transferred at $\bar{c}$, to obtain a line $\bar{\ell}'$ parallel to $\bar{\ell}$. Finally, two lines are traced through $\bar{a}$ and $\bar{c}$, which are perpendicular to $\bar{\ell}$ and $\bar{\ell}'$, respectively. The intersections of such lines with the first two lines give the other two vertices $\bar{b}$ and $\bar{d}$ of the rectangle. This construction applies to the manifold setting, too, by copying the angle in the tangent planes, as described in Section 6.5.1, and using the square set to trace perpendicular lines. However, the resulting quadrilateral has two square angles at $a$ and $c$, but nothing can be said on

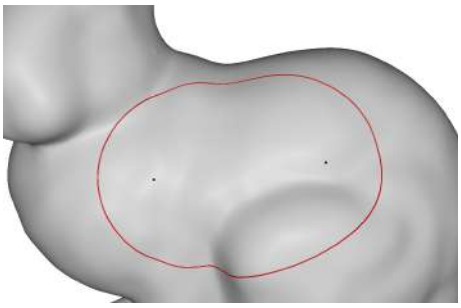

**Figure 6.15:** Ellipse (red curve) computed as an isoline of the sum of the distance fields from its foci (black dots).

the amplitude of the other two angles, and opposite edges are not congruent in general. A number of other constructions can be devised, which are all equivalent in the Euclidean setting, while none of them can warrant congruent opposite edges and four right angles. Each such construction privileges some of the properties of rectangles, at the expense of others.

Figure 6.14 shows examples of rectangles obtained with the three constructions described above.

### 6.5.5 Ellipse

An ellipse cannot be constructed using the straightedge and compass. The best one can do is to compute the position of a point on the ellipse, using the so called *de La Hire*'s construction. However, since the ellipse can be defined as an isoline of the sum of the distance fields from its foci $a$ and $b$. In details, once the foci have been chosen, we use the *Isoline* operator to compute the isoline of the field $f = d_a + d_b$ equal to $\alpha\ell$, where $\ell$ is the distance between the two foci and $\alpha$ is a scaling factor. We therefore added this primitive to our drawing system for practical reasons. An example is shown in Fig.6.15.

## 6.6 Unresolved Contructions

We could not find a straightforward way to port further constructions to a surface by relying just on the basic tools available in our arsenal. For completeness, we briefly discuss some such constructions, which may be relevant in the applications, leaving their investigation to future work.

#### Perpendicular to a line through a point not on the line

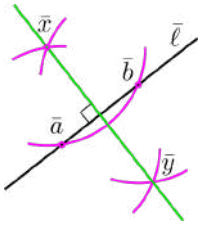


This is a basic construction, which is also useful in the context of more complex constructions in the Euclidean plane. Given a line $\bar{\ell}$ and a point $\bar{x}$ not on the line, find a line through $\bar{x}$ and perpendicular to $\bar{\ell}$. In the plane, we trace a circle centered at $\bar{x}$, with an aperture larger than its distance

from $\bar{\ell}$; we find the intersection points $\bar{a}, \bar{b}$ of this circle with $\bar{\ell}$; and we trace another two circles centered at $\bar{a}$ and $\bar{b}$ with the same aperture. The result is the line through $\bar{x}$ and $\bar{y}$.

In the geodesic setting, the orthogonal projection of a point $x$ onto a geodesic $\gamma$ in general will not be the midpoint of the segment intercepted on $\gamma$ with a circle centered at $x$. We rather have to define the problem in terms of distances: if point $z$ on $\gamma$ minimizes the distance from $x$, then the geodesic path $\gamma_{xz}$ meets $\gamma$ orthogonally at $z$, because it is a radial path of the circle centered at $x$ and tangent to $\gamma$.

This problem could be tackled by computing the distance field from $\gamma$ (which is not part of our arsenal, though) and evaluating it at $x$: the geodesic circle centered at $x$ with radius $d_\gamma(x)$ is tangent to $\gamma$ at $z$. Alternatively, one could restrict the distance field $d_x$ to $\gamma$ and find its minimum along it. Notice that both such solutions take measures, thus violating the rules of the straightedge and compass framework. A possible workaround consists of growing a geodesic circle centered at $x$ until it becomes tangent to $\gamma$. The radius of the circle can be halved or doubled by relying on the basic constructions and a bisection technique can be followed. A similar problem is mirroring a point $x$ about a line $\gamma$ not containing it. Once we have found the projection $z$ of $x$ on $\gamma$, it is sufficient to trace a circle centered at $z$ and through $x$ and then find the intersection between such circle and the geodesic line through $x$ and $z$.

### Parallel lines

A number of constructions in the plane deal with parallel lines. In the manifold setting, the concept itself of parallel lines is ill-defined. Given a geodesic line $\gamma_x$ and point on $x \in \gamma_x$, the tangent $t_x$ of $\gamma_x$ in $x$ belongs to the tangent plane $T_xS$, and it is well defined its *parallel transport* to the tangent plane $T_yS$ of another point $y \in S$. The parallel transport is a fairly complex operation that we have not considered in our preliminaries. Once the parallel transported direction $t_y$ is given, we could trace the geodesic through $y$ tangent to $t_y$ and consider it "parallel" to $\gamma_x$. The trouble here is, that the direction $t_y$ will be different depending both on the starting point $x$ on $\gamma_x$, and on the trajectory that we choose to transport $t_x$ to $T_yS$. Therefore, the result is not unique and it is somehow arbitrary. Another straightforward possibility it to take a reference line $\gamma$ and define a bundle of "parallel" lines as all those lines that intersect $\gamma$ with a given angle. Given points $x_0, \ldots, x_n$ along $\gamma$ and the reference angle, it is possible to use the construction in Section 6.5.1 to trace such parallel lines through the points $x_i$. Note that, even if we were allowed to take distances, the locus of points that have a given distance from a geodesic line $\gamma$ consists of two curves that in general are *not* geodesic lines. Addressing this problem thus requires first a robust notion of parallelism on a manifold.

| | **Tangent Space** | **Geodesic Tools** | |
|---|---|---|---|
| *Angle Bisection* | is a geodesic ✓<br>bisects the angle ✓<br>is equidistant from sides ✗ | is a geodesic ✓<br>bisects the angle ✗<br>is equidistant from sides ✗ | |
| *Segment Bisector* | is a geodesic ✓<br>bisects the segment ✓<br>is orthogonal ✓<br>is equidistant from endpoints ✗ | is a geodesic ✗<br>bisects the segment ✓<br>is orthogonal ✓<br>is equidistant from endpoints ✓ | |
| *Circle through 3 points* | ✗ | ✓ | |
| *Isoscele Triangle* | ✗ | 2 equal sides ✓<br>apex belonging to the perpendicular bisector of the base ✗ | 2 equal sides ✗<br>apex belonging to the perpendicular bisector of the base ✓ |
| *Equilateral Triangle* | equal sides ✗<br>equal angles ✗<br>radial geodesics of the same length ✓<br>angles at the center of 120° ✓ | equal sides ✓<br>equal angles ✗<br>radial geodesics of the same length ✗<br>angles at the center of 120° ✗ | |
| *Square* | equal sides ✗<br>equal angles ✗<br>radial geodesics of the same length ✓<br>angles at the center of 90° ✓<br>diagonals intersect at their midpoints ✓ | 4 equal sides ✓<br>1 right angle ✓<br>radial geodesics of the same length ✗<br>angles at the center of 90° ✗<br>diagonals intersect at their midpoints ✗ | 2 equal sides ✓<br>2 right angles ✓<br>radial geodesics of the same length ✗<br>angles at the center of 90° ✗<br>diagonals intersect at their midpoints ✗ |
| *Rectangles* | equal sides ✗<br>equal angles ✗<br>radial geodesics of the same length ✓<br>diagonals intersect at their midpoints ✓ | 4 equal sides ✓<br>1 rigth angle ✓<br>radial geodesics of the same length ✗<br>diagonals intersect at their midpoints ✗ | 2 equal sides ✓<br>2 right angles ✓<br>radial geodesics of the same length ✗<br>diagonals intersect at their midpoints ✗ |
| *Polygons* | equal sides ✗<br>equal angles ✗<br>radial geodesics of the same length ✓<br>equal angles at center (only regular ones) ✓ | ✗ | |

**Table 6.1:** Summary of the supported constructions, with the properties preserved by the algorithms described in Sec. 6.4 (Tangent Space) and in Sec. 6.5 (Geodesic Tools). Where more than one construction is available, we report the main differences between them splitting the corresponding columns. In most cases, the properties that fail with one approach are preserved by the other.

### More constructions

Several other constructions exploit relations between angles and distances, which do not hold in the manifold case. For this reason, we could not find a straightforward way to reproduce such constructions in terms of our geodesic arsenal:

- Tangents to a circle through an external point: the construction in the plane is based on the fact that an angle at the circumference in a half circle measures $\pi/2$. This is no longer true in the manifold case.
- Circle inscribed in a triangle: the construction in the plane is based on the fact that all points in the bisectors of angles are equidistant from the edges. This is no longer true in the manifold case. It is not clear how the locus of points that are equidistant from two edges can be constructed, unless the distance fields from the edges can be computed (see also the discussion in Sec. 6.5.1).

Note also that constructions like the trisection of an angle or doubling the volume of a cube are not possible using the straightedge and compass while they can be achieved by using a marked ruler. This suggests that in the manifold case, too, more constructions could be supported be allowing the explicit computation of distances from curves.

## 6.7 Implementation

All the constructions described in the previous sections, which apply to the manifold setting, have been implemented by means of the primitives defined in Section 6.3 and included as an extension of an existing library [PNC19]. We have developed a prototype system that supports their interactive usage

on meshes up to the size of millions of triangles. We refer to Chapter 3 for the definition of basic concepts such as tangent spaces and parallel transport, as well as the description of the algorithm for geodesic paths and distances computation.

DATA STRUCTURES The surface $S$ is represented with a piecewise flat triangular mesh $M$, which is represented with an indexed data structure – i.e., encoding a list of vertices $V$ and a list of triangles $F$ – augmented with triangle-to-triangle adjacencies to support mesh navigation.

A mesh point $p$ is encoded as a triple $(t, \alpha, \beta)$ where $t$ is the index of the triangle containing $p$, and $\alpha, \beta$ are two barycentric coordinates of $p$ in $t$ (while the third barycentric coordinate is computed by difference to the unit).

A curve $\gamma$ on $S$ is discretized as a polyline having vertices at all intersections with edges of $M$. A curve connecting points $p$ and $q$ is encoded with a strip of triangles $(t_0, \ldots, t_h)$ of $M$, where $t_0$ and $t_h$ contain $p$ and $q$, respectively, and an array of scalars $(l_0, \ldots, l_{h-1})$, where $l_i$ encodes the intercept of the polyline with the edge common to $t_i, t_{i+1}$ parametrized along such edge.

TANGENT Let $\gamma$ be the shortest path connecting two points $q_0, q_1$, represented as described above. Given the representation of polylines described above, the tangent vector $w_p$ at a point $p$ on $\gamma$ is computed as follows. If $p$ lies in a triangle $t_i$ then $w_p$ belongs to the plane containing $t_i$, and it is computed as $w_p = p_i - p$, with $p_i := (1-l_i)v_0 + l_i v_1$ where $v_0, v_1$ are the endpoints of the edge shared by $t_i$ and $t_{i+1}$. If $p$ belongs to an edge, we proceed in a similar way: the only difference is that $w_p$ will be of the form $p_{i+1} - p_i$, with obvious meaning of the notations. If $p$ is a vertex, we first compute $w_p$ as before, obtaining a vector defined in the plane containing a triangle $t_i$ in the one-ring of $p$. Then we map $w_p$ to the tangent space of $p$ in the same way we have mapped its neighbors.

ISOLINE We linearly interpolate a field inside each triangle of $M$. For each triangle $t$, which crosses a given isovalue, the segment of isoline crossing $t$ is computed independently. While linear interpolation is good enough on high resolution meshes, it might be too rough on coarse meshes. Better results can be achieved by supersampling the polyline while using a more accurate estimate of the distance field inside $t$. For instance, isolines can be approximated as arcs of circle in the plane containing $t$, where the center of the circle is estimated on the basis of the values of the distance field at the vertices of $t$.

INTERSECT Lines on $M$ are encoded as paths, as described before. Intersections between a pair of lines are found in linear time in the total number of triangles in the corresponding paths. Each triangle intersecting one of the paths is assigned a unique tag; next the triangles forming the other path are scanned, and intersections are computed just at tagged triangles.

CONVEXITY BALLS As already remarked, we assume that our constructions occur within a convex set. We thus provide an algorithm to test the radius of convexity about a given point $p$. This is computed by considering the largest ball $B$ centered at $p$ within which the Hessian of $d_p^2(x)$ is definite-positive for every $x \in B$. This boils down to test the positive-definiteness of $\left(\text{Hess} d_p^2\right)_{ij}$ by checking its eigenvalues while applying a growing-region procedure from $p$. Note that, while a test of convexity guarantees correctness, in practice many constructions may work well also on larger neighborhoods. Since all constructions are interactive, we leave freedom to the user to apply them over arbitrarily large regions.

ROTATION, TRANSLATION, SCALING In order to support interaction, we allow the user to edit a drawing by translating, rotating and scaling geometric objects over the surface. Geometric transformations are applied to the control points that define our constructions, while the objects are generated each time from the updated points. Given an anchor point $p$, we use the log map to represent all control points of the object at hand in the tangent plane of $p$. This is implemented point-wise by evaluating the shortest paths between $p$ and each such point, and finding the tangent of each path at $p$. Rotation and scaling are implemented trivially, by changing one of the polar coordinates of the points in tangent space: the angle for rotation and the distance for scaling. Then we map the updated points to the surface with the exp map, which is implemented point-wise by tracing geodesic lines from $p$ either in the updated directions, or with updated lengths. Translation consists of dragging the anchor point while parallel transporting the reference frame of its tangent space along the trajectory. Upon dragging, the control points are regenerated likewise from the transported frame.

For most constructions described in Section 6.4, a natural choice for the anchor point is the center $c$ where we locate the tangent space for the construction. For the remaining constructions, we select as anchor point one of the control points participating in the construction.

MACROS We provide some macro-operations, which combine different primitive constructions to obtain complex decorations at once. Some examples of macros are shown in the decorations in Figure 6.1. For instance: a *wreath* is obtained by multiple instances of a polygon rotated about the same center; similarly, we allow the user to draw *nested shapes* like circles or polygons; a *flower* is built by drawing arcs of circles centered at the vertices of a polygon and trimming them at their intersections. The *cross* and the *spider net* on the skull are also generated by macros that intersect circles. Macros are controlled interactively with simple parameters that tune, e.g., the number of polygons forming a wreath, the number of nested shapes, the number of petals in a flower, etc.

## 6.8 Concluding remarks

We have presented two approaches – namely, constructions in tangent space and direct constructions on the surface – to port straightedge and compass constructions to the manifold setting. It follows from our analysis that not all constructions can be ported successfully, and also those that can be ported may guarantee only *some* of the properties they have in the Euclidean case. We extended the scope of basic constructions by exploiting our *Distance-field* operator beyond the limitations of the straightedge and compass framework, yet remaining compatible with it, since we neither take explicit measures nor do arithmetic computations. The constructions we propose already support several operations in the context of interactive vector graphics on surfaces.

A few relevant constructions are still not supported. Such operations may require explicit measures, which are forbidden in the straightedge and compass framework and may require further tools beyond our geodesic arsenal, such as computing the distance field from a curve.

A further challenge is extending our primitives to work over larger regions. However, even basic properties of lines and circles can be lost outside strongly convex regions. See Figure 2.8 for some examples. Some operations have been addressed already in the literature, including primitives that can be computed with distance fields [NPP22], and Bézier splines [MNPP22].

A relevant limitation, stemming from the intrinsic curvature of surfaces, is the impossibility to warrant the congruence of both lengths and angles together. Regular tilings, which are hard to apply because of this limitation, can be addressed by relaxing some conditions on angles and/or lengths, but they remain challenging to extend over large regions. This problem is tightly related to the design of N-RoSy fields [VCD+17], in particular to the presence of field singularities, which cannot be avoided, as a consequence of the Gauss-Bonnet theorem.

A possible avenue is to relax the constraint of lines to be straight, in geodesic terms, trading some straightness for other properties. This leads to the concept of *as-straight-as-possible* lines under given constraints, e.g., joining their endpoints with a prescribed length or with given tangent directions. This approach entails investigating Jacobi fields [PHD+10, Le 19] and related optimization problems.

We plan to address the above challenges in future work.